Journal of Electrical Engineering, Vol. 76, No. 4, 2025, pp. 333-343

Planar rat-race couplers and Wilkinson power dividers for quad-band applications using extended Pi-shaped impedance transformers

Nguyen Minh Giang[1,*], Le Dang Manh[1], Dang Hong Hanh[2]

This paper presents a novel design for planar quad-band rat-race couplers (RRCs) and Wilkinson power dividers (WPDs). To achieve quad-band operation, a quad-band impedance transformer circuit is proposed in the form of an extended Pi-shaped structure. For demonstration purposes, prototypes of an RRC operating at 0.8/1.6/2.484/3.284 GHz and a WPD operating at 0.7/1.21/1.792/2.303 GHz were designed, fabricated, and measured. Good agreement between simulations and measurements was achieved. The measured results indicate that the RRC exhibits an insertion loss of less than 1.48 dB, isolation better than 23 dB, and input return loss exceeding 19.87 dB at four operating frequencies. Meanwhile, the quad-band WPD achieves an insertion loss of less than 0.69 dB and isolation better than 21.25 dB.

Keywords: rat-race coupler, Wilkinson power divider, quad-band, planar structure, impedance transformer

1 Introduction

Rat-race couplers (RRCs) and Wilkinson power dividers (WPDs) are essential passive components used in many RF systems such as multiplier circuits, balanced antenna systems, balanced amplifiers, and mixers. WPDs and RRCs have the same functionality of dividing the input power into component powers at the output ports with either balanced or unbalanced ratios. Compared to WPD, RRC offers certain advantages, such as the ability to handle higher input power and generate two output signals that are either in-phase or out-of-phase. However, they have the drawbacks of larger size and more ports compared to Wilkinson power dividers. Over the decades, numerous types of RRC and WPD have been proposed with enhanced features such as bandwidth expansion [1-2], size reduction [3-4], improved power division ratio [5-6], and frequency reconfigurability [7-9]. Notably, with the advancement of multi-band applications, various designs for multi-band RRC and WPD circuits have been proposed. A common method for designing multi-band RRC/WPD circuits is to utilize equivalent multi-band structures as replacements for the quarter-wavelength transmission lines in the conventional single-band RRC/WPD. In [10-11], dual-band RRC/WPD are designed based on dual-band PI-shaped and T-shaped structures. Work [12] presents a method for designing dual-band and multi-band RRCs utilizing multi-band notch filters. The main disadvantage of the method [12] is the narrow stopband between adjacent passbands. Another approach to designing dual-band and tri-band RRC/WPD is based on composite right/left-handed (CRLH) transmission lines [13-14]. However, this method requires the use of lumped elements L and C, which can lead to increased losses and parasitic effects when operating at high frequencies. A tri-band RRC and WPD are reported in [15-16] utilizing an extended T-shaped microstrip line. In [17], a tri-band WPD is designed using a three-section transmission line transformer. This method requires the use of optimization algorithms to calculate the circuit parameters.

Although there have been many publications on dual-band and tri-band RRC/WPD circuits, there are currently few publications on quad-band RRCs and WPDs. Designing these quad-band circuits requires the development of quad-band impedance transformer. When the number of frequency bands increases to four, the number of variables and equations also increases, leading to a more complex design compared to the dual-band and tri-band cases. In [18], a quad-band RRC is designed based on a developed quad-band impedance transformation structure. Then, by utilizing this quad-band structure, a quad-band WPD is designed in [19]. A compact quad-band RRC and WPD, based on the negative refractive index, were designed in [20-21]. However, these circuits utilize lumped elements and exhibit poor insertion loss and isolation. In [22], an RRC operating at four bands with suppression of spurious passbands is reported. The circuit in [22] features a two-layer structure based on a laterally offset dual ring resonator backed by concentric dual split ring slots. In [23], a quad-band WPD is designed using two cascaded sections of dual-band transformers. Another approach to designing quad-band WPD is based on SIW technologies [24], offering a compact size, good return loss. However, the main drawback of the circuit is its high insertion loss.

[1] Faculty of Radio-electronic Engineering, Le Quy Don Technical University, 100000 Hanoi, Vietnam
[2] Radar Research Department, Air Defense and Air Force Technical Institute, 100000 Hanoi, Vietnam
*giangnm@lqdtu.edu.vn

https://doi.org/10.2478/jee-2025-0034, Print (till 2015) ISSN 1335-3632, On-line ISSN 1339-309X

In this paper, a novel approach for designing planar quad-band RRCs and WPDs is proposed. The circuits are based on a novel quad-band impedance transformation structure. Unlike previously reported quad-band impedance transformers that utilize two coupled lines [18, 25], the proposed structure relies on only one coupled line, resulting in a simpler design process. Moreover, the configuration introduced in [25], which employs a coupled line short-circuited at both ends, poses greater challenges in layout design and fabrication due to the need for precise grounding and via placement, thereby increasing structural complexity and sensitivity to fabrication tolerances. The proposed circuits are designed based on the exactly developed analytical equations. To verify the effectiveness of the proposed design method, both an RRC and a WPD were designed, fabricated, and tested. The agreement between the measured and simulated results confirms the validity of the proposed method. The measurement results show that the RRC/WPD circuits exhibit low insertion losses, high isolation with good performance in terms of and return loss and phase imbalance.

2 The proposed quad-band impedance transformer

The proposed quad-band impedance transformer (QBIT) is illustrated in Fig. 1(a).

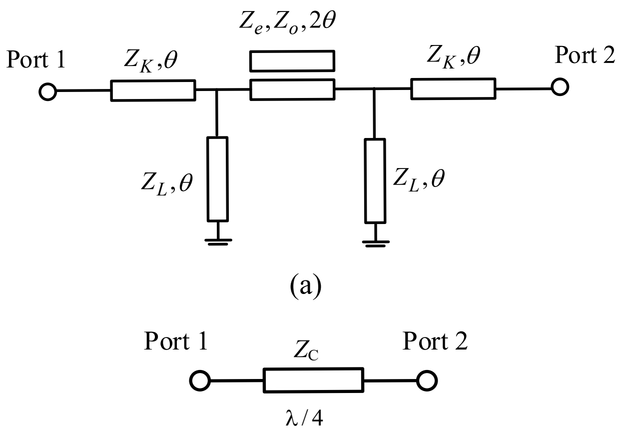

Fig. 1. (a) Proposed quad-band impedance transformer, and (b) its equivalent quarter-wavelength transmission line with characteristics impedance Z_C

The circuit has an extended Pi-shaped structure, consisting of a coupled line with an electrical length of 2θ and even- and odd-mode characteristic impedances Z_e and Z_o, two series transmission lines (Z_K, θ), and two short stubs (Z_L, θ). Parameters of the QBIT are calculated to ensure that it is equivalent to a quarter-wavelength transmission line with a characteristic impedance Z_C (Fig. 1b) at four frequency bands, the proposed impedance transformer circuit, the approach from [18] was used.

The ABCD matrix of the QBIT is determined as follows:

$$M_{QBIT} = M_K M_L M_M M_L M_K \tag{1}$$

in which

$$M_K = \begin{bmatrix} \cos\theta & jZ_K \sin\theta \\ j\dfrac{\sin\theta}{Z_K} & \cos\theta \end{bmatrix}$$

$$M_L = \begin{bmatrix} 1 & 0 \\ -j\dfrac{\cot\theta}{Z_L} & 1 \end{bmatrix}$$

$$M_M = \begin{bmatrix} \cos 2\theta & j\dfrac{Z_M \sin 2\theta}{2} \\ j\dfrac{2\sin 2\theta}{Z_M} & \cos 2\theta \end{bmatrix}$$

where $Z_M = Z_e + Z_o$.

Meanwhile, the ABCD matrix of a quarter-wavelength transmission line with characteristic impedance Z_C is determined as follows

$$M_C = \begin{bmatrix} 0 & jZ_C \\ \dfrac{j}{Z_C} & 0 \end{bmatrix}$$

To make the QBIT equivalent to a transmission line, the following conditions must be satisfied:

$$M_K M_L M_M M_L M_K = \pm M_C \tag{2}$$

From (2) we derive

$$M_L M_M M_L = \pm M_K^{-1} M_C M_K^{-1} \tag{3}$$

From (3), the following conditions are derived:

$$\tan^2\theta \pm \left(\frac{Z_K^2 + Z_C^2}{Z_K Z_C}\right)\tan\theta - \left(1 + \frac{Z_M}{Z_L}\right) = 0 \tag{4}$$

$$\tan^2\theta \pm \frac{Z_M Z_C}{Z_K^2}\tan\theta - \frac{Z_C^2}{Z_K^2} = 0 \tag{5}$$

For the QBIT and transmission line Z_C to be equivalent at four frequency bands, Eqns. (4) and (5) must be identical and have four solutions, namely θ_1, θ_2, θ_3, and θ_4. These are electrical lengths corresponding to four operating frequencies f_1, f_2, f_3, and f_4. From this, we have:

$$Z_M = \frac{Z_K(Z_K^2 + Z_C^2)}{Z_C^2} \tag{6}$$

$$Z_L = \frac{Z_K^3}{Z_C^2}\left(\frac{Z_C^2 + Z_K^2}{Z_C^2 - Z_K^2}\right) \tag{7}$$

$$\theta_1 = \tan^{-1}\left[\frac{Z_C}{Z_K}\left(\sqrt{1+\frac{(Z_K^2+Z_C^2)^2}{4Z_C^4}}-\frac{Z_K^2+Z_C^2}{2Z_C^2}\right)\right] \quad (8)$$

The remaining electrical lengths are determined as follows:

$$\theta_2 = \tan^{-1}\left[\frac{Z_C}{Z_K}\left(\sqrt{1+\frac{(Z_K^2+Z_C^2)^2}{4Z_C^4}}+\frac{Z_K^2+Z_C^2}{2Z_C^2}\right)\right] \quad (9)$$

$$\theta_3 = \pi - \theta_2 \quad (10)$$

$$\theta_4 = \pi - \theta_1 \quad (11)$$

Since frequency is proportional to electrical length, we have the following relationships

$$\frac{f_2}{f_1}=\frac{\theta_2}{\theta_1},\ \frac{f_3}{f_2}=\frac{\theta_3}{\theta_2}=\frac{\pi}{\theta_2}-1,\ \frac{f_4}{f_1}=\frac{\theta_4}{\theta_1}=\frac{\pi}{\theta_1}-1 \quad (12)$$

Using the derived equations, the QBIT can be designed. Suppose we need to design QBIT to match Z_A to Z_B at four frequency bands. The design procedure for the QBIT circuit is summarized as follows:

Step 1. Calculate characteristic impedance Z_C of the quarter-wavelength transmission line to match impedance Z_A to Z_B according to equation [26]:

$$Z_C = \sqrt{Z_A Z_B} \quad (13)$$

Step 2. Replace the quarter-wavelength transmission lines Z_C with an equivalent QBIT. Parameters of the QBIT are calculated as follows:

2.1. Select the frequencies f_1 and f_4
2.2. Using (12) to define θ_1
2.3. By substituting θ_1 and Z_C into (8), Z_K is determined
2.4. Substituting Z_K and Z_C into (9) allows θ_2 to be calculated
2.5. Determine operating frequencies f_2 and f_3 from (12)
2.6. From (6)-(7), determine the values of Z_M and Z_L

The following sections will present the design method for quad-band RRCs and quad-band WPDs based on the proposed QBIT.

3 Design method of quad-band RRC based on QBIT

3.1 The proposed quad-band RRC

The conventional RRC is presented in Fig. 2 [26].

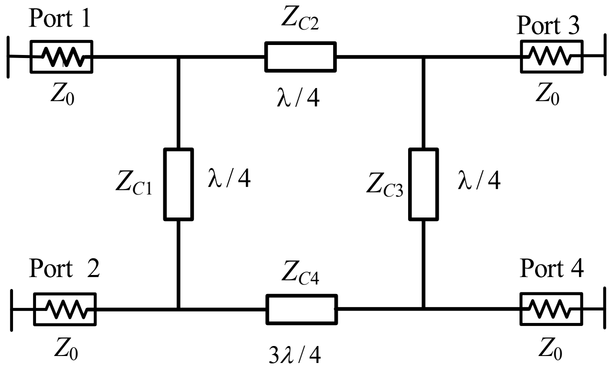

Fig. 2. Conventional single-band RRC [26]

It consists of four transmission lines Z_{C1}, Z_{C2}, Z_{C3}, and Z_{C4} with the same characteristic impedance 70.71 Ω. Except for the transmission line Z_{C4}, which has an electrical length of $3\lambda/4$, the other three transmission lines all have the same electrical length of λ/4.

To enable the conventional RRC to operate at four frequency bands, three quarter-wavelength transmission lines Z_{C1}, Z_{C2}, and Z_{C3} are replaced with their corresponding QBIT structures. As for the transmission line Z_{C4}, due to its electrical length of 3λ\4, it is divided into three transmission lines Z_{C41}, Z_{C42}, and Z_{C43}, each with an electrical length of λ/4. These transmission lines will also be replaced with their corresponding QBIT structures. Thus, the proposed quad-band RRC configuration is shown in Fig. 3. Parameters of the QBIT are calculated based on the procedure outlined in Section 2 so that the QBIT is equivalent to a quarter-wavelength transmission line with a characteristic impedance of Z_C=70.71 Ω.

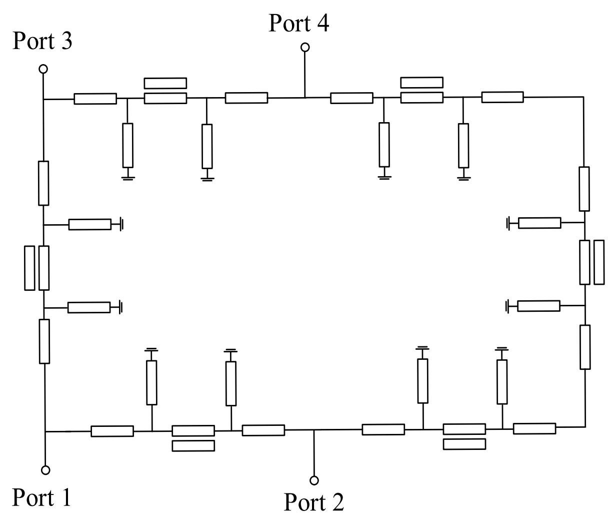

Fig. 3. The proposed quad-band RRC based on QBIT

Next, we will examine the fabrication limitation of the quad-band RRC. For the circuit to be manufacturable using normal printed circuit board (PCB) technology, the characteristic impedances Z_K and Z_L must fall within the range 15 Ω ≤ Z_K, Z_L ≤ 120 Ω. From (7), we have:

$$15\ \Omega \leq \frac{Z_K^3}{Z_C^2}\left(\frac{Z_C^2+Z_K^2}{Z_C^2-Z_K^2}\right) \leq 120\ \Omega \qquad (14)$$

Substituting Z_C=70.71 into Eqn. (14), we obtain:

$$35.514\ \Omega \leq Z_K \leq 54.026\ \Omega \qquad (15)$$

Substituting Z_K into (6), we derive:

$$44.474\ \Omega \leq Z_M \leq 85.564\ \Omega \qquad (16)$$

Substituting Z_K into (8), we obtain:

$$32.3° \leq \theta_1 \leq 47.8° \qquad (17)$$

Using (11), we derive:

$$132.2° \leq \theta_4 \leq 147.7° \qquad (18)$$

From (12), it follows that:

$$2.765 \leq \frac{f_4}{f_1} \leq 4.566 \qquad (19)$$

Similarly, by determining the electrical length θ_2 from (9) and substituting it into (12), we obtain:

$$1.418 \leq \frac{f_3}{f_2} \leq 1.581 \qquad (20)$$

Thus, equations (19) and (20) define the frequency ratio constraints of the proposed quad-band RRC circuit.

3.2 Design and implementation of quad-band RRC

To validate the proposed design methodology, a quad-band RRC operating at 0.8/1.6/2.484/3.284 GHz has been designed, fabricated, and tested on a Rogers RO4003C substrate, which features relative permittivity 3.55 and a thickness of 0.813 mm. By applying the design procedure of QBIT outlined in Section 2, parameters of the scheme are calculated as follows. Initially, the frequencies f_1=800 MHz and f_4=3.284 GHz are selected. These frequencies are then substituted into Eqn. (13), resulting in the electrical length θ_1=35.26°. Using Eqns. (9) and (10), the values of Z_K and θ_2 are determined as Z_K=50.2 Ω and θ_2=70.52°, respectively. Furthermore, from (13), the remaining operating frequencies f_2 and f_3 are calculated as f_2=1.6 GHz and f_3=2.484 GHz. Finally, substituting Z_K and Z_C=70.71 Ω into Eqns. (6) and (7) yields Z_M=75.05 Ω and Z_L=75.17 Ω. From the value of Z_M, we can select any values of Z_e and Z_o such that Z_e+Z_o= Z_M and Z_e >Z_o. Note that a large difference between Z_e and Z_o will result in a very small spacing between the two transmission lines of the coupled line, making fabrication difficult. In this case, we choose Z_e=40 Ω, Z_o=35.05 Ω. Based on the calculated results, the circuit layout was designed. Figure 4 illustrates the physical layout diagram of the designed RRC.

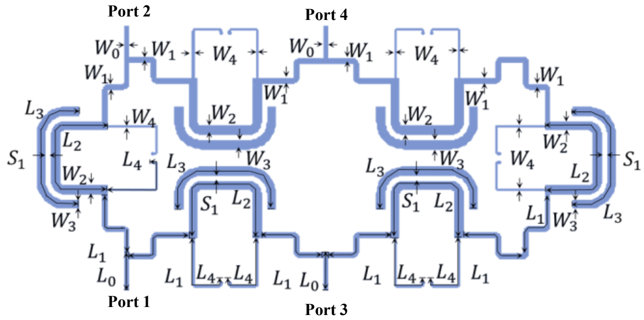

Fig. 4. Physical layout diagram of the designed quad-band RRC

Dimensions of the RRC circuit sections are shown in Table 1.

Table. 1. Detail design parameters of the quad-band RRC

Dimension	Value (mm)	Dimension	Value (mm)
L_0	9	W_0	1.78
L_1	21.99	W_1	1.78
L_2	46.11	W_2	2.74
L_3	42.96	W_3	2.74
L_4	22.63	W_4	0.84
S_1	1.41		

Figure 5 illustrates the fabricated quad-band RRC and experimental setup.

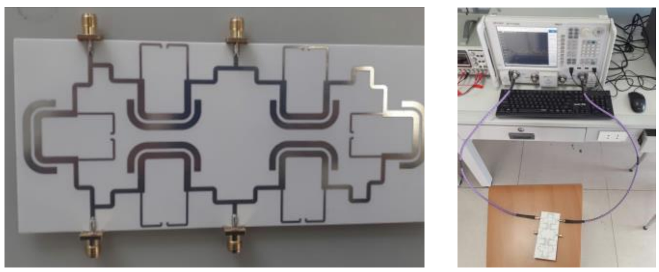

Fig. 5. The fabricated quad-band RRC and experimental setup

Figure 6 shows the measured and simulated $|S_{21}|$, $|S_{31}|$, and $|S_{11}|$ parameters of the fabricated quad-band RRC when the input signal is applied to port 1, output signals are obtained from ports 2 and 3, and port 4 functions as the isolation port.

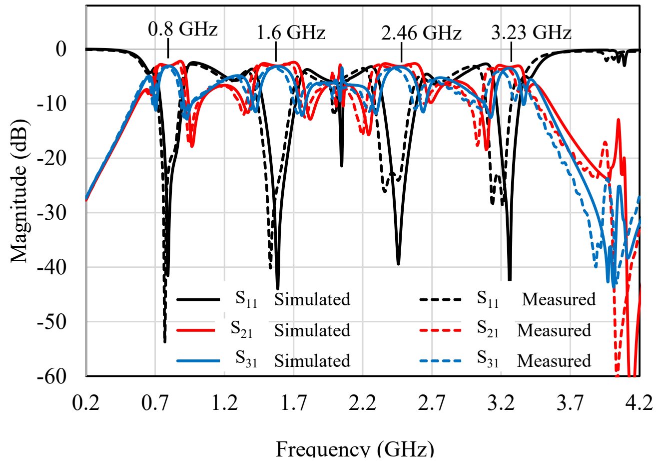

Fig. 6. Simulated and measured parameters S_{21}, S_{31}, and S_{11} of the proposed quad-band RRC

From Fig.6, it can be observed that the measured results align well with the simulated ones, and the fabricated RRC operates at four center frequencies: 0.8 GHz, 1.6 GHz, 2.46 GHz, and 3.23 GHz. The slight shift in the center frequencies, which becomes especially noticeable at higher frequencies, is primarily influenced by transmission line discontinuities, including T-junction and bend discontinuities. Additionally, the difference in even- and odd-mode phase velocities due to the non-ideal shape of the coupled line segments also contributes to this deviation. To minimize the frequency deviation, the layout was refined using smooth transitions to suppress reflection and phase distortion. Full-wave electromagnetic simulations, including realistic discontinuities and substrate effects, were employed. Slight tuning of stub lengths and coupling gaps further improved the agreement between measurements and simulations. Collectively, these measures reduced the center-frequency error to a minimal level at all bands, bringing measurements into close agreement with simulations. From Fig. 6, it can be observed that at the four center frequencies, the insertion losses at ports 2 and 3 are 3.23/3.11/3.32/3.73 dB and 3.44/3.77/3.82/4.43 dB, respectively. Thus, compared to the ideal value of 3 dB, the insertion losses at the ports do not exceed 1.43 dB. Moreover, Fig. 6 clearly shows that the input return loss |S11|at the four operating frequencies is better than 21.4 dB.

Figure 7 shows the measured and simulated results of the phase difference $\angle S_{21} - \angle S_{31}$. When the input signal is applied to port 1, the theoretical value of the phase difference $\angle S_{21} - \angle S_{31}$ is 0º.

From Fig.7, we can see that the measured results agree well with the simulations. The detailed measured data indicate that at the four operating frequencies of 0.8/1.6/2.46/3.23 GHz, the phase differences $\angle S_{21} - \angle S_{31}$ are 4°, 5.34°, 3.7°, and 2.2°, respectively. Thus, compared to the theoretical value of 0°, the measured phase differences exhibit relatively small deviations, all within 5.34°.

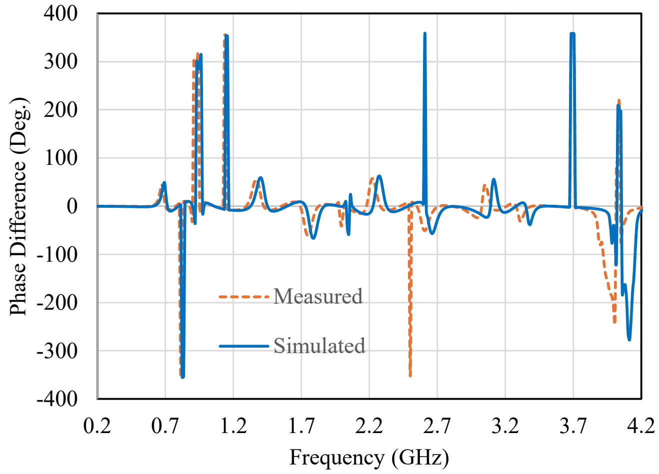

Fig. 7. Simulated and measured phase difference $\angle S_{21} - \angle S_{31}$

Figure 8 illustrates the simulated and measured scattering parameters $|S_{24}|$, $|S_{34}|$, and $|S_{44}|$ of the designed quad-band RRC when the input signal is applied to port 4. From Fig. 8, it can be observed that the measured results agree well with the simulated ones. At the four operating frequencies of 0.8/1.6/2.46/3.23 GHz, the insertion losses at ports 2 and 3 are 3.47/3.72/3.78/4.48 dB and 3.4/3.3/3.56/4.44 dB, respectively. Meanwhile, the return loss $|S_{44}|$ at all four frequencies is better than 19.87 dB.

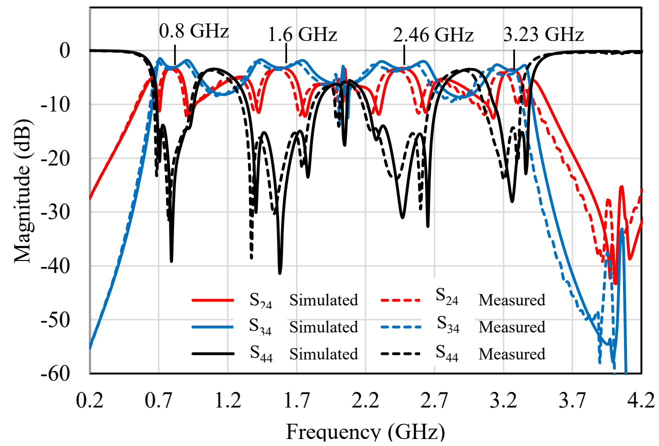

Fig. 8. Simulated and measured parameters S_{24}, S_{34}, and S_{44} of the proposed quad-band RRC

From Figs. 6 and 8, it is clear that no significant unexpected spurious passbands are observed beyond the fourth band. In the out-of-band regions (above 3.7 GHz and below 0.3 GHz), the transmission coefficient remains well suppressed to nearly –20 dB, confirming that the circuit provides strong rejection outside the intended bands.

The measured isolation level between ports 1 and 4 is presented in Fig. 9. The measured results indicate that the isolation S_{41} achieves good performance at the four operating frequencies, with values all above 23 dB.

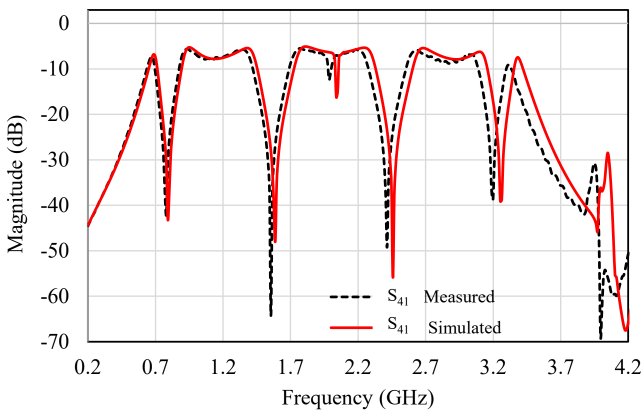

Fig. 9. Simulated and measured parameter S_{41} of the proposed quad-band RRC

Next, the measured phase difference $\angle S_{24} - \angle S_{34}$ is presented in Fig.10.

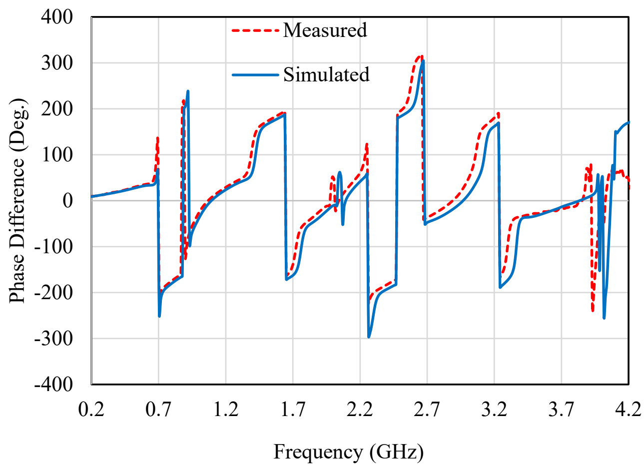

Fig. 10. Simulated and measured phase difference $\angle S_{24} - \angle S_{34}$

The measured results in Fig. 10 show that the phase deviation $\angle S_{24} - \angle S_{34}$ at the 4 operating frequencies are 174.6° / 187.3° / 186.5° / 172.33°. Thus, compared to the theoretical value of 180°, the measured results exhibit a relatively small phase deviation. Comparison between the performance of the proposed quad-band RRC and other works is presented in Table 2.

Tab. 2. Comparison between the measured performance of the proposed quad-band RRC and other works

Reference	[14]	[22]	[20]	[27]	This work
Frequency	0.195/0.65/ 1.415	1.45/3.8/ 4.3/6.3	0.9/1.55/ 2.017/2.55	0.71/1.64/ 4.09/5.03	0.8/1.6/ 2.46/3.23
Type	Tri-band, BLC	Quad-band, RRC	Quad-band, RRC	Quad-band, BLC	Quad-band, RRC
IL (dB)	< 1.67	< 3.3	< 3.37	< 1.83	< 1.48
IRL (dB)	> 19.62	> 18.2	> 10	> 18.18	> 19.87
IS (dB)	> 18.24	> 30	> 10	> 17.92	> 23
PD (°)	< 2	< 8	NI	< 7	< 7.7
Size ($\lambda_g \times \lambda_g$)	0.045×0.045	0.5×0.7	NI	0.2×0.2	0.39×0.87
FBW (%)	NI	NI	NI	28.6/5/1.6/2/1.96	11.3/7.7/6.7/3.6

In Table 2, IRL, IS, IL, and PD represent input return loss, isolation, insertion loss, and phase difference, respectively, measured at the operating frequencies; λ_g is guided wavelength at frequency f_1; BLC represents branch-line coupler; NI means no information. FBW denotes the fractional bandwidth. The FBW is determined based on the criterion that the amplitude differences between the two output ports remain within 1 dB for the first and second bands and within 1.5 dB for the third and fourth bands.

From the comparison table, it can be observed that the proposed RRC circuit demonstrates superior isolation and insertion loss, while maintaining good performance in terms of return loss and phase difference. Additionally, compared to the circuit in [22] with a two-layer structure and the circuits in [14, 20] utilizing lumped L and C elements, the proposed circuit features a simpler design.

4 Design method of quad-band RRC based on QBIT

4.1 Proposed quad-band WPD

The traditional Wilkinson power divider is illustrated in Fig.11[26].

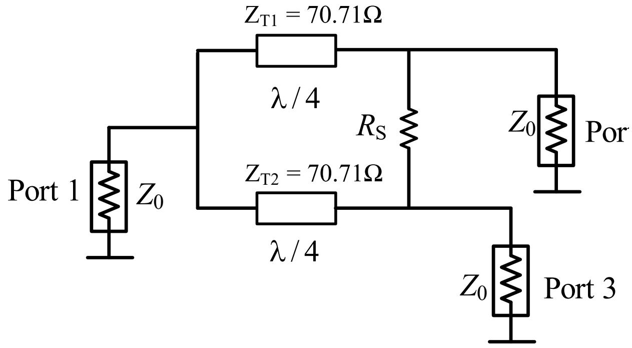

Fig. 11. Traditional single-band WPD

The circuit consists of two quarter-wavelength branches Z_{T1} and Z_{T2}, each with the same characteristic impedance $Z_{T1}=Z_{T2}=50\sqrt{2}\,\Omega$. An isolation resistor R_S=100 Ω is connected between the two branches to ensure isolation and impedance matching at the two output ports, 2 and 3.

To design a WPD operating at four frequency bands, the quarter-wavelength transmission lines Z_{T1} and Z_{T2} of the conventional single-band WPD are replaced with their equivalent QBITs. The quad-band WPD circuit is illustrated in Fig. 12.

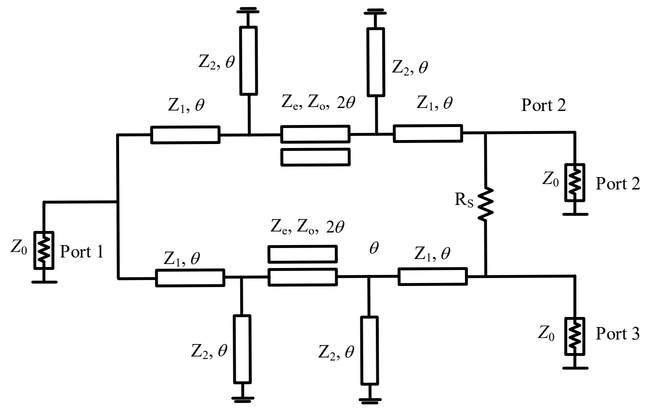

Fig. 12. Proposed quad-band WPD based on QBIT

The QBIT are calculated based on the design procedure presented in Section 2 to ensure their equivalence to quarter-wavelength transmission lines with an impedance of Z_T = 70.71 Ω at the four desired operating frequencies.

Since the quad-band WPD and quad-band RRC circuits are both designed based on replacing the quarter-wavelength transmission line with characteristics impedance of 70.71 Ω with a QBIT, the design limitations (19) and (20) of the quad-band RRC circuit presented in Section 3 also serve as the design constraints for the quad-band WPD.

4.2 Design and implementation of quad-band WPD

To confirm the validity of the design method, a quad-band WPD with operating frequencies f_1= 0.7 GHz, f_2 =1.21 GHz, f_3 =1.792 GHz, and f_4 = 2.303 GHz has been designed, fabricated, and measured. The circuit is designed on Rogers RO4003C material with a relative dielectric constant of 3.55 and a thickness of 0.813 mm. By applying the design procedure presented in Section 2, the design parameters of the circuit are calculated as follows: $\theta=\theta_1$=41.96°, θ_2=72.56° Z_1=41.79 Ω, Z_M=56.39 Ω, and Z_2=30.27 Ω. The values of Z_e and Z_o are selected as Z_e=29.39 Ω, Z_o=27 Ω.

Based on the calculated parameters, the layout of the quad-band WPD was designed (Fig. 13).

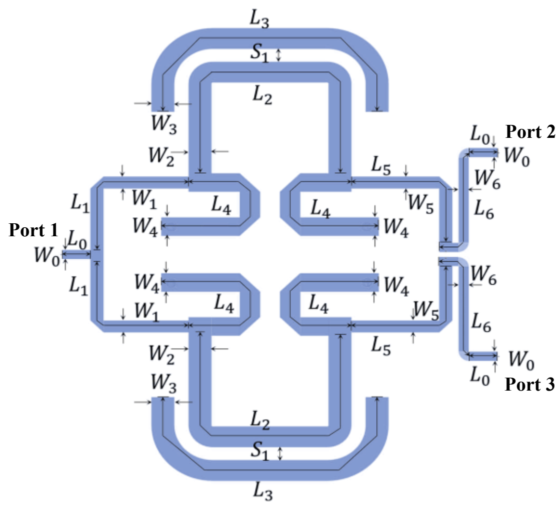

Fig. 13. Physical layout diagram of the designed quad-band WPD

Details design parameters of the WPD circuit are provided in Table 3.

Table 3. Detail design parameters of the quad-band WPD

Dimension	Value (mm)	Dimension	Value (mm)
L_0	15	W_0	1.78
L_1	59.78	W_1	4.86
L_2	29.26	W_2	4.96
L_3	30.16	W_3	1.78
L_4	31.08	W_4	1.78
S_1	2.51		

The fabricated quad-band WPD is shown in Fig. 14. The fabricated quad-band WPD has a size of 77 mm × 94 mm.

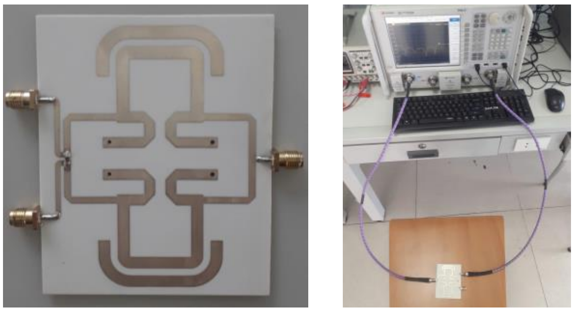

Fig. 14. Fabricated quad-band WPD and experimental set up

Figure 15 illustrates the measured and simulated results of the $|S_{21}|$ and $|S_{31}|$ parameters of the designed quad-band WPD.

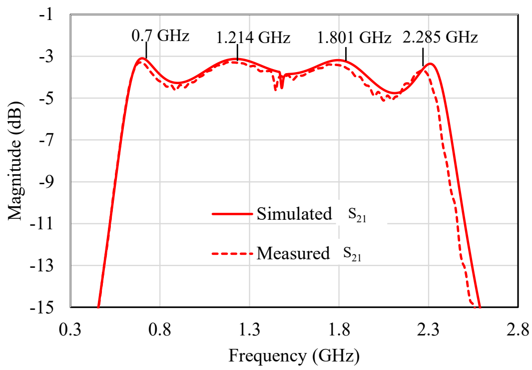

(a)

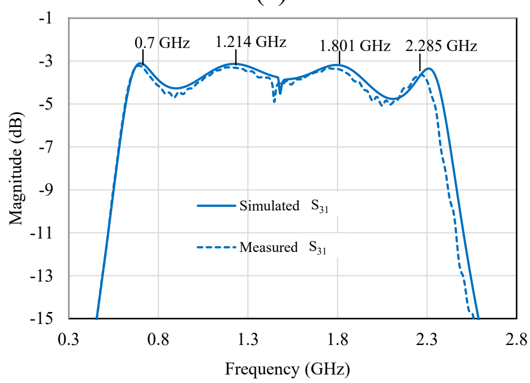

(b)

Fig. 15. (a) Measured and simulated parameters S_{21}, and (b) S_{31} of the proposed quad-band WPD

From Fig. 15, it is evident that the results show good agreement between measurement and simulation, with the four center operating frequencies identified as 0.7 GHz, 1.214 GHz, 1.801 GHz, and 2.285 GHz. The measured insertion losses at ports 2 and 3 for these frequencies are 3.27/3.21 dB, 3.24/3.27 dB, 3.4/3.36 dB, and 3.69/3.68 dB, respectively. These values agree well with the theoretical insertion loss of 3 dB, with errors not exceeding 0.69 dB. Besides, as illustrated in Fig. 15, the transmission coefficients $|S_{21}|$ and $|S_{31}|$ remain well suppressed outside the operating bands, particularly below 0.4 GHz and beyond 2.5 GHz, with levels typically below –15 dB. This demonstrates strong signal rejection and the absence of undesired spurious passbands below the first band and beyond the fourth band. The lack of spurious transmission peaks confirms that the proposed WPD offers high frequency selectivity and effectively confines signal propagation within the designated frequency bands.

Figures 16 and 17 present the measured and simulated return losses and isolation of the designed PD.

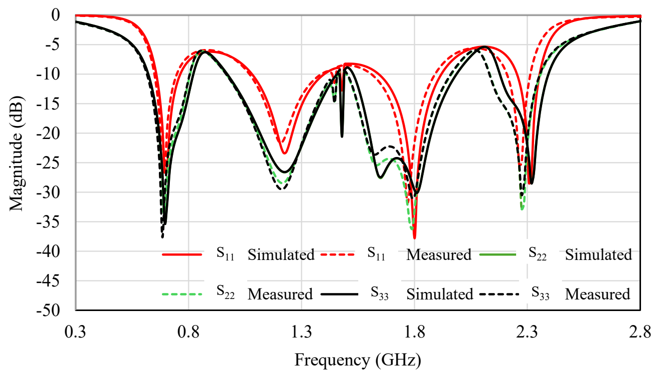

Fig. 16. Measured and simulated parameters S_{11}, S_{22}, and S_{33} of the proposed quad-band WPD

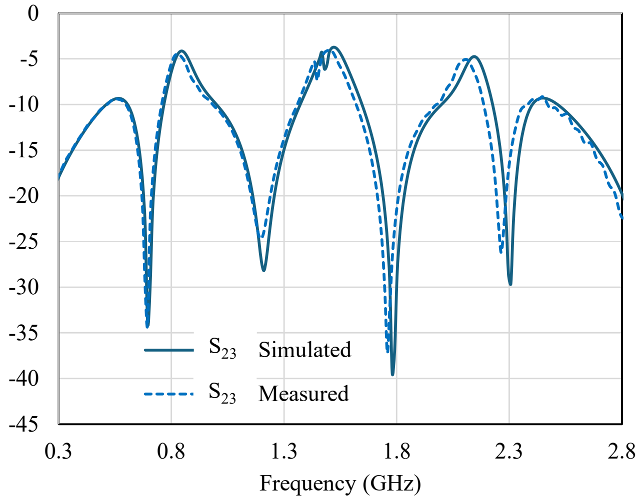

Fig. 17. Measured and simulated isolation parameters S_{23} of the proposed quad-band WPD

It can be seen that the simulation results closely match the measurements. Additionally, the isolation between the two output ports exceeds 21.25 dB, while the return losses are better than 20.6 dB at the four operating bands.

Next, in Figs. 18 and 19, the measured results of amplitude imbalance (AI) and phase imbalance (PI) of the proposed quad-band WPD are presented.

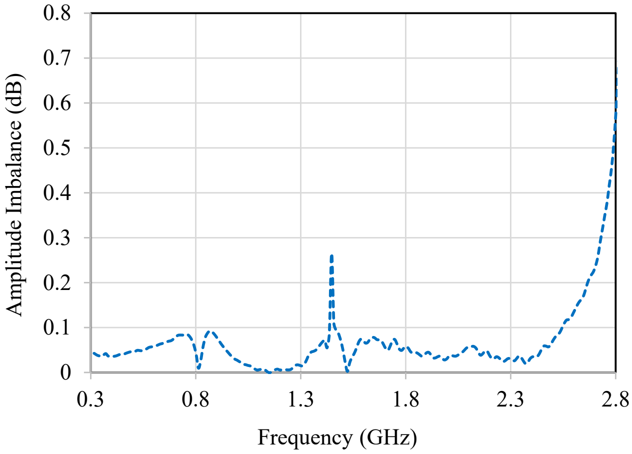

Fig. 18. Measured amplitude imbalance of the proposed quad-band WPD

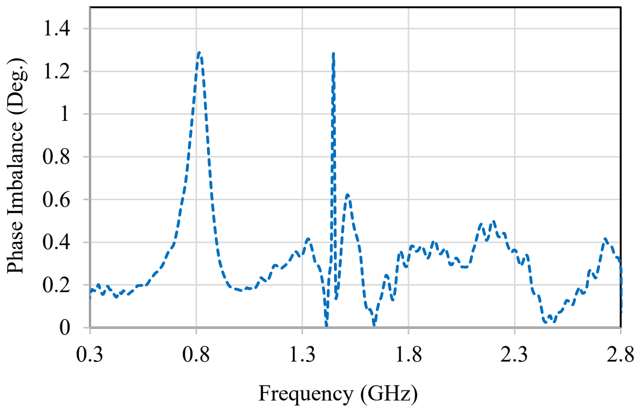

Fig. 19. Measured phase imbalance of the proposed quad-band WPD

It can be observed that over the wide frequency range of 0.3 GHz to 2.8 GHz, the AI and PI values remain very low, with AI being less than 0.5 dB and PI less than 1.3°. At the four operating frequencies of 0.7 GHz, 1.214 GHz, 1.801 GHz, and 2.285 GHz, the AI values are below 0.06 dB, and the PI values are below 0.35°.

Table 4 presents a comparison of the measured parameters of the fabricated quad-band WPD with those of other works.

Tab. 4. Comparison between the measured performance of the proposed quad-band WPD and other reported works

Reference	Frequency (GHz)	IL (dB)	IS (dB)	RL (dB)	Size ($\lambda_g \times \lambda_g$)	FBW (%)
[19]	0.7/1.2/ 1.78/2.28	< 0.75	> 20.92	> 18.14	0.33 ×0.39	NI
[24]	3.34/4.82/ 6.17/7.66	< 1.85	> 10.7	> 19.2	0.12×0.24	NI
[23]	2.1/2.5/ 3.5/3.8	< 0.6	> 11	> 15	0.07×0.13	NI
[28]	2.4/3.5/ 5.2/5.8	< 1.2	> 16	> 18	NI	NI
[29]	0.5/1.3/ 2.2/3	< 2	NI	> 19	NI	NI
[30]	0.898/1.78/ 2.712/3.581	< 0.95	> 28.6	NI	0.163×0.167	12.7/16/ 11.3/2.8
This work	0.7/1.214/ 1.801/2.285	< 0.69	> 21.25	> 20.6	0.34×0.41	7.2/11.9/ 7.6/2.2

Here, FBW denotes the fractional bandwidth. The FBW of the proposed PD circuit and the circuit in [30] is determined based on the criterion that all return losses and isolation are better than 15 dB.

From Tab. 4, it is clear that the major advantage of the proposed circuit is its lower insertion loss compared to previously published designs, with a value not exceeding 0.69 dB at the four operating frequencies. Additionally, other critical parameters, including isolation and return loss, are well maintained at levels exceeding 20.6 dB and 21.25 dB, respectively. The circuit in [23], although exhibiting low insertion loss, suffers from poor isolation and return loss.

5 Conclusions

This paper presents a novel approach to designing quad-band RRCs and WPDs based on a proposed quad-band impedance transformer. To validate the design methodology, both RRC and WPD prototypes were fabricated and experimentally tested. The measured results show good agreement with simulations, exhibiting excellent transmission, matching, and isolation performances, which confirm the reliability of the proposed method. Specifically, the RRC demonstrates an insertion loss of less than 1.48 dB, isolation better than 23 dB, and return loss exceeding 19.87 dB at four operating frequencies. Meanwhile, the WPD achieves insertion loss below 0.69 dB and isolation better than 21.25 dB. The amplitude imbalance and phase imbalance are less than 0.06 dB and 0.35°, respectively, at the four operating frequencies These characteristics make the proposed structures highly suitable for multi-band microwave systems.

References

[1] Y. Zheng, W. Wang, Y. Yang and Y. Wu, "Single-Layer Planar Wideband Rat-Race Coupler Using a Shorted Parallel-Coupled Multi-Line Section," *IEEE Transactions on Circuits and Systems II: Express Briefs*, vol. 67, no. 12, pp. 3053–3057, 2020.

[2] A. Chen, Y. Zhuang, J. Zhou and Y. Huang, "Design of a Broadband Wilkinson Power Divider with Wide Range Tunable Bandwidths by Adding a Pair of Capacitors," *IEEE Transactions on Circuits and Systems II: Express Briefs*, vol. 66, no. 4, pp. 567–571, 2019.

[3] W. Nie, S. Luo and Y. X. Guo, "Miniaturized Rat-Race Coupler with Harmonic Suppression," *IEEE Microwave and Wireless Components Letters*, vol. 24, no. 11, pp. 754–756, 2014.

[4] Z. F. Jin, J. Xu, M. Zhao and Y. Liu, A Compact Wideband Lumped-Element Wilkinson Power Divider Using Inverting Coupled Coil, *IEEE Microwave and Wireless Technology Letters*, vol. 34, no. 6, pp. 599602, 2024.

[5] H. R. Ahn and S. Nam, Wideband Microstrip Coupled-Line Ring Hybrids for High Power-Division Ratios, *IEEE Transactions on Microwave Theory and Techniques*, vol. 61, no. 5, pp. 17681780, 2013.

[6] X. Yang and D. H. Hong, A 4-GHz 1:10 Unequal Wilkinson Power Divider Using Split Ring Resonator, in 2017 3rd *IEEE International Conference on Computer and Communications (ICCC)*, Chengdu, China, 2017, pp. 27182721.

[7] X. Tan, J. Sun and F. Lin, A Compact Frequency-Reconfigurable Rat-Race Coupler, *IEEE Microwave and Wireless Components Letters*, vol. 30, no. 7, pp. 665 668, 2020.

[8] X. Tan and F. Lin, A Novel Rat-Race Coupler with Widely Tunable Frequency, *IEEE Transactions on Microwave Theory and Techniques*, vol. 67, no. 3, pp. 957–967, 2019.

[9] B. Wu, Z. Sun, X. Wang and Y. Liu, □A Reconfigurable Wilkinson Power Divider with Flexible Tuning Range Configuration, *IEEE Transactions on Circuits and Systems II: Express Briefs*, vol. 67, no. 7, pp. 1219□1223, 2020.

[10] A. Majeed and M. Ashraf, "Dual-Band Ring Couplers Using T- and Π-Section," *International Journal of Microwave and Optical Technology*, vol. 3, pp. 460–466, 2008.

[11] A. Sahu, K. A. Al Shamaileh, P. H. Aaen and M. S. Hashmi, "A High-Frequency/Power Ratio Wilkinson Power Divider Based on Identical/Non-Identical Multi-T-Sections with Short-Circuited Stubs," *IEEE Open Journal of Circuits and Systems*, vol. 2, pp. 34–45, 2021.

[12] X. Yang, J. W. Xie, X. C. Zhang and Y. Liu, "Novel Multiband Ring Coupler Based on Notch Filter," *International Journal of RF and Microwave Computer-Aided Engineering*, vol. 30, no. 8, e22394, 2020.

[13] I. H. Lin, M. Devincentis, C. Caloz and T. Itoh, "Arbitrary Dual-Band Components Using Composite Right/Left-Handed Transmission Lines," *IEEE Transactions on Microwave Theory and Techniques*, vol. 52, no. 4, pp. 1142–1149, 2004.

[14] Q. Wang, J. Lim and Y. Jeong, "Design of a Compact Tri-Band Branch Line Coupler Using Double-Lorentz Composite Right/Left-Handed Transmission Lines," *Microwave and Optical Technology Letters*, vol. 59, no. 2, pp. 304–308, 2017.

[15] Q. X. Chu and F. Lin, "A Novel Tri-Band Rat-Race Coupler with T-Shape Step Impedance Transformers," *Microwave and Optical Technology Letters*, vol. 52, no. 6, pp. 1240–1244, 2010.

[16] C. Miao, B. Li, G. Yang and Y. Liu, "Design of Unequal Wilkinson Power Divider for Tri-Band Operation," *Progress in Electromagnetics Research Letters*, vol. 28, pp. 159–172, 2012.

[17] M. Chongcheawchamnan, S. Patisang, M. Krairiksh and I. D. Robertson, "Tri-Band Wilkinson Power Divider Using a Three-Section Transmission-Line Transformer," IEEE Microwave and Wireless Components Letters, vol. 16, no. 8, pp. 452–454, 2006.

[18] A. Althuwayb, "Design of a Quad-Band Rat-Race Coupler for GSM/WiMAX/WLAN/Satellite Applications," *Radioengineering*, vol. 30, pp. 135–141, 2021.

[19] N. M. Giang, L. H. M. Thang, L. D. Manh and T. T. T. Nguyen, "A Simple Design of Low-Loss Quad-Band Wilkinson Power Dividers," *Journal of Electrical Engineering*, vol. 75, pp. 63–71, 2024.

[20] A. Papanastasiou, "Design and Implementation of Quad-Band Microwave Devices Using the Negative Refractive Index Transmission-Line Technique," Ph.D. dissertation, Dept. of Electrical and Computer Engineering, University of Cyprus, Nicosia, Cyprus, May 2015.

[21] A. C. Papanastasiou, G. E. Georghiou and G. V. Eleftheriades, "A Quad-Band Wilkinson Power Divider Using Generalized NRI Transmission Lines," *IEEE Microwave and Wireless Components Letters*, vol. 18, no. 8, pp. 521–523, 2008.

[22] S. Velan, S. Kingsly, M. Kanagasabai and R. S. Kumar, "Quad-Band Rat-Race Coupler with Suppression of Spurious Pass-Bands," *IEEE Microwave and Wireless Components Letters*, vol. 26, pp. 490–492, 2016.

[23] A. M. El-Tager, A. M. El-Akhdar and H. M. El-Hennawy, "Analysis of Coupled Microstrip Lines for Quad-Band Equal Power Dividers/Combiners," *Progress in Electromagnetics Research B*, vol. 41, pp. 187–211, 2012.

[24] N. C. Pradhan, K. S. Subramanian, R. K. Barik and S. K. Koul, "Design of Compact Substrate Integrated Waveguide Based Triple- and Quad-Band Power Dividers," *IEEE Microwave and Wireless Components Letters*, vol. 31, no. 4, pp. 365–368, 2021.

[25] R. K. Barik, K. V. P. Kumar and S. S. Karthikeyan, "Design of a Quad-Band Branch Line Balun Using Extended Pi-Shaped Coupled Lines," *IEEE Microwave and Wireless Components Letters*, vol. 26, pp. 771–773, 2016.

[26] D. M. Pozar, *Microwave Engineering*, 4th ed., New York: Wiley, 2012.

[27] G. Wu, S. Qi, W. Liu and B. Hu, "A Quad-Band Branch Line Coupler with High Frequency Ratio," *IEICE Electronics Express*, vol. 19, no. 3, p. 20210487, 2022.

[28] H. Younesiraad, M. Bemani and M. Fozi, "A Novel Fully Planar Quad-Band Wilkinson Power Divider," *AEU – International Journal of Electronics and Communications*, vol. 74, pp. 75–82, 2017.

[29] H. H. Jaradat, N. I. Dib and K. A. Al Shamaileh, "A Compact Coplanar Waveguide Quad-Band Wilkinson Power Divider Using Non-Uniform Transmission Lines," in *2019 International Applied Computational Electromagnetics Society Symposium (ACES)*, Miami, FL, USA, 2019, pp. 1–2.

[30] B. Xia, L. S. Wu, J. Mao and Y. Liu, "A New Quad-Band Wilkinson Power Divider," *Journal of Electromagnetic Waves and Applications*, vol. 28, no. 13,

Received 13 April 2025